

Laurent Ponson and Elisabeth Bouchaud

Fracture Mechanics of Heterogeneous Materials

A Statistical Approach



Contents

- 1 Elements of fracture mechanics** *1*
- 2 Rupture and microstructure** *13*
- 3 Fracture of thin sheets** *29*
 - 3.1 Experimental observations *29*
 - 3.1.1 Geometry of crack profiles *31*
 - 3.1.2 Acoustic emission *33*
 - 3.2 Crack path predictions in 2D heterogeneous materials *34*
 - 3.2.1 Perfectly brittle cracks *34*
 - 3.2.2 The role of damage on crack trajectory *38*
- 4 Roughening and intermittency of interfacial cracks: failure as a depinning transition** *43*
- 5 Fracture in three-dimensional solids: how to decipher fracture surfaces** *57*
- 6 Effective toughness of heterogeneous brittle materials** *77*

3

Fracture of thin sheets

Before describing fracture in all its complexity, *i.e.* fracture of a fully three-dimensional material, we will restrict, in this chapter, to the rupture of quasi-bidimensional materials, *i.e.* thin sheets. "Thin" means of course that the thickness of the considered sample - hardly exactly zero in the real world! - is much smaller than any other dimension. If the sample is perfectly homogeneous, this simply means that its thickness has to be much smaller than its length and width. But if it contains a certain amount of disorder associated to a characteristic scale, then the thickness has to be smaller, or, at the most, of the order of this new length. Hence, a one centimeter thick piece of nanocrystalline metal cannot be considered to be two-dimensional, while a one centimeter thick piece of expanded polystyrene with grains of a few millimeters in size is a good approximation for what will be called a "thin sheet" below.

3.1

Experimental observations

In this context, the simplest fracture experiment one can think of is the tearing of a paper sheet. Heterogeneities in paper are more or less tightly connected cellulose fibers, which are typically (for common paper) $20\ \mu\text{m}$ in diameter and 1 to 2 mm in length. Hence, sheets which are one tenth of a millimeter thick - a few fiber diameters only - can be considered as a good approximation of a two-dimensional material. However, let us note that for a two-dimensional system, all the components of the displacement field should be contained within the sheet plane, which is usually not the case. In other words, it is extremely difficult to perform tearing in pure mode I. The out-of-plane displacement of the paper ahead of the propagating crack, leading to mixed mode failure, is visible in Fig. 3.1.

Whatever the mode however, two basic observations can be made when paper is torn. During the experiment, noise can be heard under the form of bursts of various intensities. One may wonder how the amplitude and the time distribution of these acoustic events can be described and related to the dynamics of the fracture process. The second observation concerns the morphology of the crack line: one can observe with naked eyes that the crack does not form a straight line, but progresses in zigzag.



Figure 3.1 A crack propagating in paper. The crack emerging from the straight notch is rough to the eye. One can also distinguish a large damaged zone where the crack is partially closed at some points. Although the material can be considered as two-dimensional, the loading conditions are 3D, as evidenced by the out-of-plane displacement of the sheet, visible on the picture.



Figure 3.2 A crack line in paper observed at three different magnifications. Apart from the fibers which are more and more visible when the magnification is increased, the crack line is very similar at the various scales.

This zigzag, however, has a specific character, since it seems to be the same when the scale of observation is changed (Fig.3.2). These two observations can hardly be described by Linear Elastic Fracture Mechanics as it was introduced in Chapter 1. The very origin of the roughness of the crack, as well as of the intermittent character of its propagation, resides in the presence of inhomogeneities. We will see that deciphering these complex phenomena will pave the way to a quantitative understanding of the role of microstructure on failure processes. This is why we will focus particularly on the understanding of roughening and intermittency in fracture in thereafter.

Fibers can indeed be seen popping out of the torn sheet in Fig.3.3, when the crack line is observed at high magnification. According to their size, their surrounding and their orientation with respect to the direction of the applied stress, fibers are more or less easy to break. A fiber may be stronger than its neighbours, or it may be oriented in such a way that it is able to pin the crack tip at a given position for some time, until there is an increase of the local stress. This is why the crack progression is not even, but proceeds through bursts of various amplitudes. Moreover, heterogeneities tend to impose local shear stresses even if the external load is purely mode I, which leads the crack to deviate locally from its nominal straight trajectory. Shear and tensile local stresses are further modified by the rough geometry of the crack itself.

We will focus first on the quantitative description of the morphology of cracks in

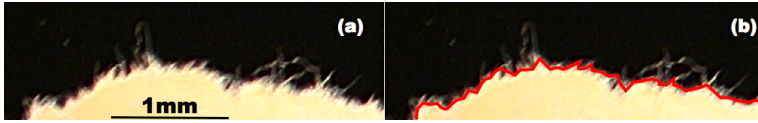


Figure 3.3 A crack line in paper observed at large magnification. (a) Fibers can be seen to pop out of the rough crack line, sometimes creating overhangs. (b) A red overlay was superimposed to the observed crack line, which does not take into account the presence of the fibers, and erases the overhangs.

thin sheets.

3.1.1

Geometry of crack profiles

The first experiment where the morphology of a crack line in paper was analyzed is due to Kertész and coworkers [1]. More recently, Salminen et al. [2] have performed similar experiments using remarkably long samples. Mallick et al. performed even more accurate statistical analysis [3].

The first step always consists in extracting a line from pictures similar to those shown in Fig. 3.1 or Fig. 3.2. At large enough scales (low magnifications), where fibers, branchings and overhangs cannot be seen, this operation is straightforward. But at smaller scales, it is not an easy task: as in Fig. 3.3(b), one has to define the envelope of the actual profile (the envelope is superimposed to the real profile in red in the figure), and obviously loose information.

Once this is done, and one deals with a rough line which can be described by a function h defined everywhere along the x axis, one can compute, for example, the second moment of the height distribution $\Delta h(\delta x)$ (see Annex 2 for details):

$$\Delta h(\delta x) = \langle (h(x + \delta x) - h(x))^2 \rangle_x^{1/2} \quad (3.1)$$

where $\langle \rangle_x$ denotes an average over all possible origins x of a window of width δx extending between x and $x + \delta x$.

For a self-affine profile, this quantity scales with δx as δx^H , where H is the Hurst, or roughness exponent. Several other momenta of the distribution of heights can be computed as well, which have, in principal, an identical behaviour (see Annex 2).

Figure 3.4 shows $\Delta h(\delta x)$ for three different kinds of paper: cardboard, drawing paper and fax paper. One can see that the exponent does not vary with the nature of the material, while the the scaling domain clearly depends on it, extending from a tenth of millimeter to an upper cutoff $\xi = 7, 1$ or 4 cm.

We have also broken a large (~ 50 cm) and thin (~ 1 cm) plate made of beads of expanded polystyrene (Fig. 3.5). The beads have a diameter of $\sim 3 - 4$ mm, so that this material belongs to the category of bidimensional specimens.

The second moment of the height distribution is shown in Fig. 3.6. Here again, the

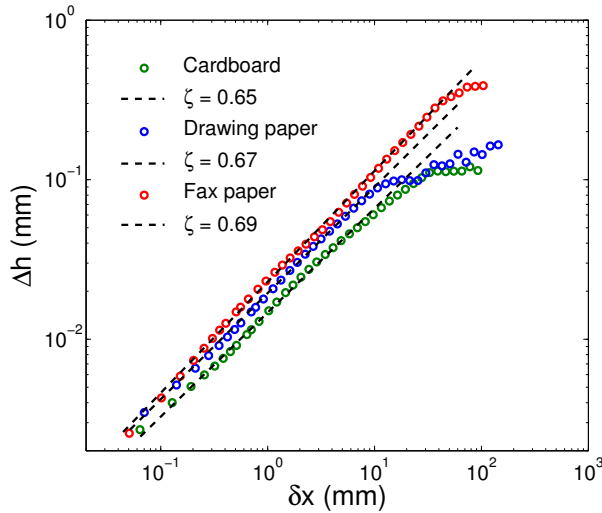


Figure 3.4 Second moment of the height distribution computed along crack lines in three different kinds of paper: cardboard (○), drawing paper (○) and fax (○) papers. In each case, $\Delta h(\delta x)$ is well fitted by a power law, with an exponent $\zeta \simeq 0.65 - 0.7$ which is very weakly dependent on the nature of the sample. The extent of the scaling domain, on the contrary, depends on the kind of paper used, and if the lower bound is of the order of a tenth of millimeters, the upper bound is 7 cm, 1 cm and 4 cm for cardboard, drawing paper and fax paper, respectively.

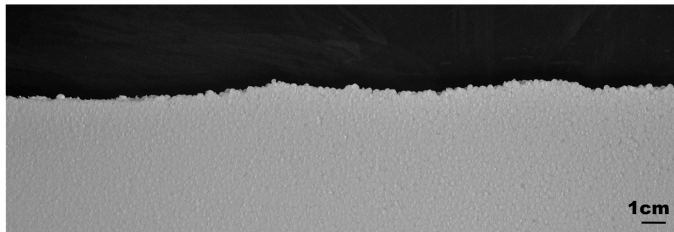


Figure 3.5 Broken specimen made of expanded polystyrene beads.

best fit of the data is a power law, which extends from the bead size (3 – 4 mm) to an upper limit $\xi \simeq 10$ cm. However, the Hurst exponent is significantly smaller than for paper, $H \simeq 0.45$. We will argue later that this exponent is indeed different, and that it is indeed the directed random walk exponent $H_{RW} = 0.5$.

In Section 3.2, we will see how to make sense of these observations. Before turning to theory, however, let us examine the other striking aspect of fracture, related to acoustic emission.

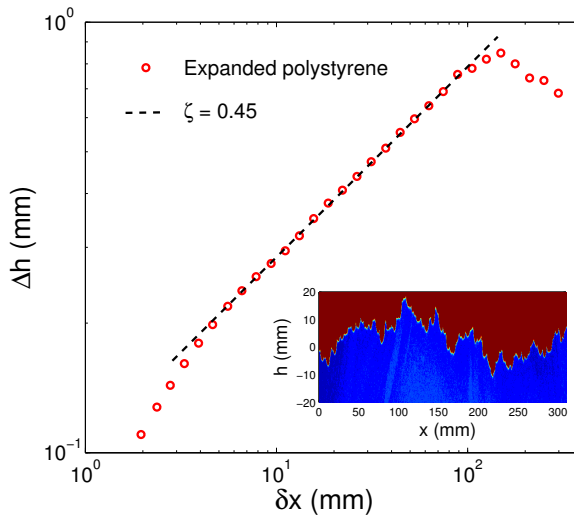


Figure 3.6 Scaling properties of cracks in expanded polystyrene. In a domain extending approximately from the bead size (3 to 4 mm) to $\xi \simeq 10$ cm, the second moment of the height distribution is well fitted by a power law with exponent $H \simeq 0.45$. *Inset:* Crack profile on which the statistical analysis was made.

3.1.2

Acoustic emission

Another striking feature of the paper tearing experiment is the complex dynamics of the failure process. A closer look at the tip of the crack shows that its motion is highly discontinuous and is made of a series of sudden jumps. This jerky motion can be characterized through the study of the acoustic emission during the failure process (Fig 3.7). These acoustic events are the signature of microinstabilities during which elastic energy is abruptly released and dissipated within the process zone. An example of acoustic signal recorded during the tearing of a sheet of paper is shown on Fig. 3.7. The events span over a broad range of amplitudes as revealed by the histogram of acoustic energies. The distribution follows a power law with exponent $\alpha \simeq 1.3$ [4], that is compatible with the statistics of crack length jumps measured locally at the crack tip [5]. Intermittent dynamics of crack with power law distributed fluctuations is a characteristic feature of the effect of disorder on failure phenomena. An interpretation of this behavior will be given in the following.

In the following section, we will present a few simple models which extend LEFM to heterogeneous materials by taking explicitly into account microstructural disorder. We will examine in particular their predictions in terms of acoustic emission and crack roughness.

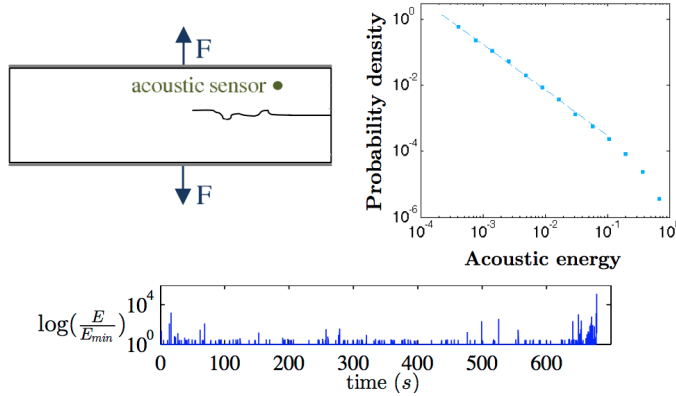


Figure 3.7 Acoustic emission during paper tearing (from Ref. [5])

3.2

Crack path predictions in 2D heterogeneous materials

In this section, we present theoretical arguments aimed at predicting the morphology of crack paths in heterogeneous specimens. The first model we are presenting derives directly from continuum mechanics, and applies to a perfectly elastic material containing some amount of disorder. Our conclusion will be that in this case, the crack path simply follows a random walk. This random walk is only altered when a microcrack or a cavity such as the ones seen in Chapter 2 opens ahead of the crack tip.

3.2.1

Perfectly brittle cracks

The model we present here is based on the principal of local symmetry [6, 7] discussed in Chapter 1: a crack follows the path along which it is loaded in pure mode I. In other words, a crack propagates along the direction with vanishing shearing mode II.

We follow the idea first introduced by Katzav et al. [8], and start from the calculation of Amestoy and Leblond [9] that predicts the propagation direction θ of a crack from the local values $k_I(x)$ and $k_{II}(x)$ of the stress intensity factors at the crack tip located in x (see Fig. 3.8):

$$\theta(x^+) = -2 \frac{k_{II}(x)}{k_I(x)} \quad (3.2)$$

We approximate the crack path as a succession of elementary straight segments separated by an incremental step δa along the x direction that can be subsequently taken in the limit $\delta a \rightarrow 0$. As a result, in Eq. (3.2), the angle $\theta(x^+)$ provides the propaga-

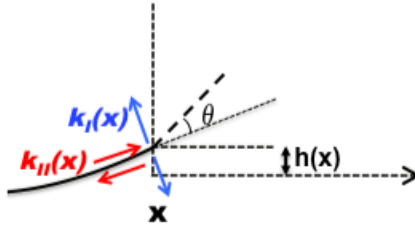


Figure 3.8 Sketch of the principle of local symmetry: the crack direction changes by an angle θ in order to annul the shearing mode II.

tion direction on the right side of the position x while the local stress intensity factors $k_I(x)$ and $k_{II}(x)$ are calculated from the crack path configuration before propagation. Since the angle θ is generally very small ($\theta \ll 1$), it can be approximated by (Fig. 3.8):

$$\theta(x^+) \simeq \frac{dh}{dx}|_{x^+} - \frac{dh}{dx}|_{x^-}. \quad (3.3)$$

To predict the crack trajectory $h(x)$, and close the system of equations (3.2) and (3.3), the local stress intensity factors are expressed as a function of the crack geometry $h(x)$ and the loading conditions. As long as the crack perturbations are small with respect to the specimen macroscopic size, one can use Cottrel and Rice's result [7] enriched by the work of Movchan *et al.* [10] that provide $\{k_I, k_{II}\}$ as a function of $h(x)$ and the stress intensity factors $\{K_I^{(0)}, K_{II}^{(0)}\}$ as well as the coefficients $\{T^{(0)}, A^{(0)}\}$ of the higher order terms in the development of the stress field ahead of the crack tip ¹⁾:

$$\begin{cases} k_I^{\text{hom}}(x) &= K_I^{(0)} \\ k_{II}^{\text{hom}}(x) &= K_{II}^{(0)} + \frac{1}{2} \frac{dh}{dx}|_{x^-} - \sqrt{\frac{2}{\pi}} T^{(0)} \int_{-\infty}^x \frac{\frac{dh}{dx}|_u}{\sqrt{x-u}} du - \sqrt{\frac{\pi}{2}} A^{(0)} h(x). \end{cases} \quad (3.4)$$

We consider cracks under macroscopic tensile loading conditions, so that $K_{II}^{(0)} = 0$ in the following.

Combining Eqs. (3.2), (3.3) and (3.4), one obtains a closed form of the path equation that writes as

$$\frac{dh}{dx}|_{x^+} = \frac{2\sqrt{2}}{\sqrt{\pi}} \frac{T^{(0)}}{K_I^{(0)}} \int_{-\infty}^x \frac{\frac{dh}{dx}|_u}{\sqrt{x-u}} du + \sqrt{2\pi} \frac{A_I^{(0)}}{K_I^{(0)}} h(x). \quad (3.5)$$

This equation holds for a homogeneous elastic medium only, and predicts a straight crack trajectory $h(x) = 0$ as long as the T -stress is negative [7].

1) The constants $\{K_I^{(0)}, K_{II}^{(0)}, T^{(0)}, A^{(0)}\}$ contain the relevant information on the specimen geometry and the loading conditions. See Chapter 1 for their definition.

To take into account the effect of spatial variations in the fracture properties of the material, one introduces the parameter $\delta k_{II}^{\text{het}} = -K_I^{(0)}\eta(x)/2$ that describes local shearing perturbations induced by the material microstructure. Taking into account both terms $k_{II} = k_{II}^{\text{hom}} + k_{II}^{\text{het}}$ in the derivation of the path equation (3.2), one obtains

$$\frac{dh}{dx}|_{x^+} = \eta(x) - \frac{c_T}{\sqrt{L_T}} \int_{-\infty}^x \frac{\frac{dh}{dx}|_u}{\sqrt{x-u}} du + c_A \frac{h(x)}{L_A} \quad (3.6)$$

where $L_T = \left(\frac{K_I^{(0)}}{T^{(0)}}\right)^2$ and $L_A = \frac{K_I^{(0)}}{A_I^{(0)}}$ are characteristic length scales of the specimen and the macroscopic loading while c_T and c_A are dimensionless constants. For example, in the Griffith geometry where a crack of length $2c$ is embedded in an infinite specimen submitted to an uniform tensile loading σ_∞ , the crack length serves as the characteristic macroscopic length scale with $L_T = L_A = c$, while the constants can be shown to take the values $c_T = \frac{2\sqrt{2}}{\pi}$ and $c_A = \frac{3}{4}$ [11].

For large enough specimens or for sufficiently long crack propagation distances, the last two terms on the right hand side of the path equation (3.6) proportional to $\sim \frac{1}{\sqrt{L_T}}$ and $\sim \frac{1}{L_A}$ vanish, while the first term $\eta(x)$ that describes the material microstructure remains independent of these characteristic lengths. This observation results in the following Langevin equation

$$\frac{dh}{dx}|_{x^+} \simeq \eta(x). \quad (3.7)$$

that predicts that the fluctuations of propagation direction are essentially the same as the fluctuations of failure properties at the microscopic scale.

This prediction can be tested directly from the original path equation (3.6) that is solved numerically in the Griffith crack geometry. Assuming the existence of a typical microstructural length scale ξ (e.g. grain diameter, fiber length...) beyond which correlations of failure properties decay exponentially fast, one predicts

$$\langle \eta(x + \delta x) \times \eta(x) \rangle_x = e^{-\left(\frac{\delta x}{\xi}\right)^2} \Rightarrow \left\langle \frac{dh}{dx}|_{x+\delta x} \times \frac{dh}{dx}|_x \right\rangle_x = e^{-\left(\frac{\delta x}{\xi}\right)^2}. \quad (3.8)$$

The autocorrelation function of the local crack propagation direction obtained numerically from Eq. (3.6) is shown in the inset of Fig. 3.9 and compares well with the one of the material disorder. The absence of correlations over distances $\delta x > \xi$ larger than the microstructural length implies that the crack follows a random walk, characterized by the Hurst exponent $\zeta = 1/2$, as predicted numerically in the context of the Griffith crack configuration (Fig. 3.9). This result is fairly consistent with the experiments on condensed polystyrene that is an archetype of 2D brittle disordered medium.

Random walk-like crack paths can also be observed in more complex microstructures. For example, intergranular failure of 2D brittle polycrystal obtained numerically using cohesive zone models result in crack trajectory with roughness exponent $H = 0.5$ (see Fig. 3.10). The lower cut-off is provided here by the microstructural length scale, the grain diameter d . In these numerical experiments, the crack cohesive

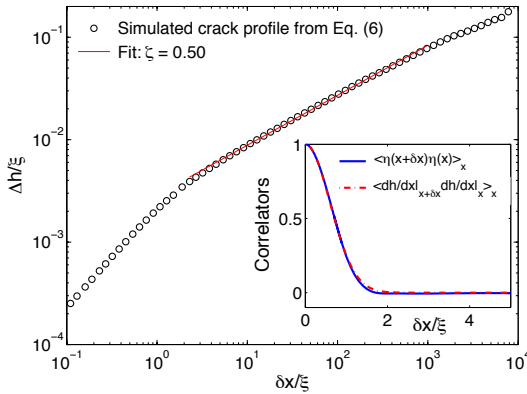


Figure 3.9 Properties of crack profiles in disordered 2D media, as predicted from Eq. (3.6): the crack follows a random walk with exponent $H = 1/2$. For very large specimens, the autocorrelation function of the local slope shown in inset is very close to the one of the material disorder η , as expected from Eq. (3.7).

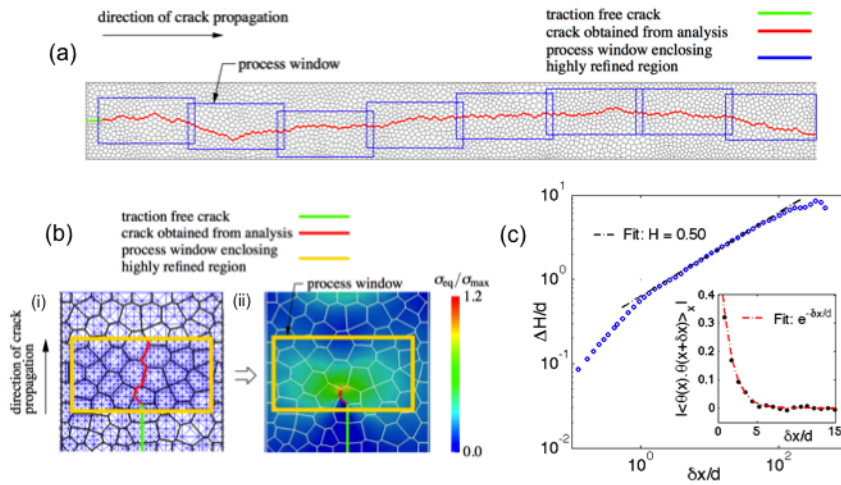


Figure 3.10 Simulated intergranular failure of polycrystals: (a) Typical example of calculated crack path; (b) Illustration of the principle of the simulations based on a finite element model of the elastic grains, separated by weak interfaces modeled using cohesive zone approach [12, 13]; (c) The crack path shows a self-affine geometry with exponent $H = 0.50$ characteristic of a random walk, and reminiscent of the brittle failure mechanism into play.

zone, or process zone size ℓ_{PZ} , where energy dissipation takes place, is smaller than the grain size d [12, 13]. This intergranular failure mode is not without reminding the process of crack propagation between the beads of expanded polystyrene shown on Fig. 3.5. There also, actual failure processes take place at a microscopic scale much smaller than the bead diameter, so that the condition $\ell_{PZ} < d$ is also fulfilled. The same fracture surface statistics with $H = 0.5$ is observed in these two very different systems where the propagation of a brittle crack is the dominant failure mechanism. This suggests the condition $\ell_{PZ} < d$ for observing brittle failure in thin sheets. This represents also the application conditions of the model of brittle failure proposed in Sec. 3.2.

Situations where the process zone is sufficiently important, so that it is larger than the typical microstructural length scale is now investigated. We will see in the next section that damage produces a different crack path statistics.

3.2.2

The role of damage on crack trajectory

A qualitative investigation: Influence of a single microcrack on crack path

In order to explore the behavior of cracks in presence of damage, we consider first a simplified configuration with one macrocrack in interaction with one microcrack. As shown in the scheme of Fig. 3.11, a very long crack, parallel to the x -axis, is preceded by a small microcrack of length $2c$ comprised within the same plane, in $-c < x < c$. The specimen is submitted to tensile loading at infinity, and we want to determine the effect of the presence of the microcrack on the behavior of the main crack. Since both cracks, in this simplified collinear geometry, will propagate within the mean fracture plane, we are interested here by the value of the stress intensity factor K_I at the tip of the main crack, and its relation with the stress intensity factor $K_I^{(0)}$ in the absence of damage.

In order to compute the stress intensity factor resulting from the presence of the microcrack, we follow the procedure proposed by Kachanov that allows for the stress field in an elastic medium with multiple cracks [14]. The main hypothesis of the technique lies in the two step procedure for the calculation of K_I . First, we consider the effect of the macrocrack on the loading conditions of the microcrack. And then, we calculate the effect of the microcrack on the macrocrack.

First, we calculate the loading conditions applying on the microcrack. We assume that the effect of the remote loading on the microcrack is negligible, because in the vicinity of the main crack tip, the effect of the stress field $\sigma_{yy}^{\text{macro}}(x)$ produced by the main crack is much larger. This stress is approximated by its homogeneous value p_0 ($\sigma_{yy}^{\text{macro}}(x)_{-c < x < c}$)

$$p_0 = \frac{1}{2c} \int_{-c}^c \frac{K_I}{\sqrt{2\pi(c+2d-x)}} = \frac{K_I}{\sqrt{\pi}} \left(\sqrt{1+d/c} - \sqrt{d/c} \right) \quad (3.9)$$

We have used here an important result for elasticity problem based on superposition

theorem [15]: loading conditions applied far away from a crack embedded in an elastic medium can be replaced by an internal pressure $p(x)$ applying on the lips of the crack, using $p(x) = \sigma_{yy}^{(nc)}(x)$ where the $\sigma_{yy}^{(nc)}(x)$ is calculated for the same geometry without crack under the same loading conditions.

In a second step, we calculate the stress field generated by the microcrack. For a crack loaded by a constant internal pressure p_0 , one gets [11]

$$\sigma_{yy}^{\text{micro}} = \frac{p_0}{\sqrt{\left(\frac{x}{c}\right)^2 - 1} \left(\frac{x}{c} + \sqrt{\left(\frac{x}{c}\right)^2 - 1}\right)} \quad \text{for } |x| > c. \quad (3.10)$$

The contribution of this stress field to the stress intensity factor of the main crack is noted $K_I^{(1)} \ll K_I^{(0)}$ and can be calculated using the classical formula $K_I = \sqrt{\frac{2}{\pi}} \int_{c+2d}^{\infty} \frac{\sigma_{yy}^{\text{micro}}(x)}{\sqrt{x-2d-c}} dx$ [16]. It follows that

$$K_I^{(1)} = \sqrt{2\pi} K_I (\sqrt{1+d/c} - \sqrt{d/c}) I_0$$

(3.11)

with $I_0 = \int_{2d/c+1}^{\infty} \frac{du}{\sqrt{u(u^2-1)}(\sqrt{u^2-1}+u)}$

The overall stress intensity factor at the tip of the main crack results then from the combined effect of the external loading and the retroactive effect of the microcrack, that can be inferred from Eqs. (3.11)

$$K_I = K_I^{(0)} + K_I^{(1)} = \frac{K_I^{(0)}}{1 - \frac{\sqrt{2}}{\pi} I_0 (\sqrt{1+d/c} - \sqrt{d/c})}. \quad (3.12)$$

Since the integral I_0 is a positive constant, the actual stress intensity factor in presence of a microcrack is actually larger than its value without it. The variations of the amplification factor $K_I/K_I^{(0)}$ as function of the cracks separation distance d/c relative to the microcrack length is represented in Fig. 3.11. The closer the cracks, the larger the interaction effects. On contrary, when the cracks are far enough, for a distance $d \simeq c$ of the order of the microcrack length, the two cracks do not interact. This is a key feature of multiple crack problems, where cracks can attract – but also repulse in some configurations – as their separation distance is of the order of their size, or smaller. Here, the process of interaction between collinear cracks results in a rapid coalescence into one single crack.

Let us now discuss the effect of damage through microcracking on the trajectory of cracks. We need to consider two steps: (i) First, microcracks find their origin in the presence of weak zones in the material. These defects, when close enough to the crack tip, are immersed in a strong tensile field. This results in the nucleation of a microcrack. As the level of tensile stress is maximum along the direction $\theta = 0$ ahead of the crack (see Fig. 3.8), microcracks are likely to be also nucleated in this direction. (ii) When a microcrack nucleates ahead of the macrocrack, new mechanism as the one described in the previous paragraph where parallel cracks were shown to attract

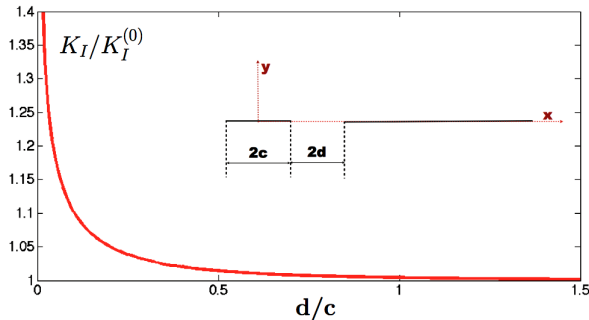


Figure 3.11 Interaction between a macro and a microcrack: The actual stress intensity factor K_I at the tip of the main crack is larger than the one $K_I^{(0)}$ without microcrack. This attraction between parallel crack vanishes for distance d larger than the microcrack length c .

each other come into play. Indeed, the main crack is now more likely to propagate in direction of the microcrack while the microcrack is more likely to propagate towards the main crack, but in the opposite direction.

This local process of crack propagation direction results in macroscopic crack paths with rather different properties than in brittle media. Indeed, this mechanism results in a persistent motion of the crack path, where excursions of crack path towards the upper $\frac{dh}{dx} > 0$ (resp. lower $\frac{dh}{dx} > 0$) direction will be more likely followed by a positive (resp. negative) local propagation direction. Contrary to a random walk where the sign of the local slopes are uncorrelated along the crack path (see *e.g.* on Fig. 3.10 in the context of a crack in a brittle polycrystal), the local slopes are positively correlated in the presence of damage. For such a persistent Brownian motion, we expect the roughness exponent to be larger than $1/2$ [17].

Before considering extensive damage, let us consider now briefly the effect of a ductile cavity on a bidimensional crack path.

Coupling between a macrocrack and a plastic cavity

In the same spirit as what we have just done by considering the trajectory of a main crack when it is preceded by a microcrack, Bouchbinder and Procaccia [18] have considered the case of a crack in front of which a cavity has opened. They consider a material which is plastic, in the Von Mises sense, *i.e.* that yields when a certain combination of the principal stresses corresponding to the distortional energy reaches a given value σ_Y , the yield stress. This defines a plastic zone, where they assume that a plastic cavity can nucleate. Actually, they suppose that this event occurs as far as possible from the crack tip, on the border of the plastic zone, which is disputable since for plastic materials, cavity nucleation is much more likely to happen within the plastic region. But this is somewhat a detail which does not compromise the generality of the result, as long as cavity nucleation takes place in an angular cone ahead

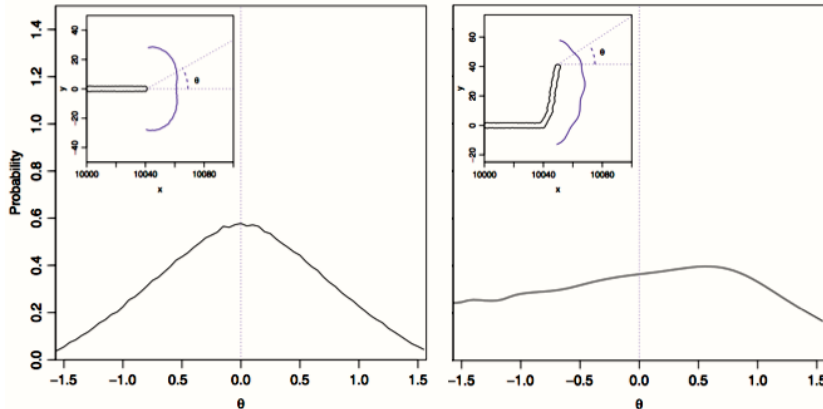


Figure 3.12 Effect of a ductile cavity on the crack path. Calculation of the elastic stress field ahead of the crack tip (left) for a straight crack (right) for a kinked crack shows that the probability of microcrack nucleation is skewed towards the positive values of direction θ in the second case. This results into a persistent behavior for the crack evolution.

of the crack tip. By computing exactly the elastic stress field thanks to a conformal invariant approach [19], they were able to show that the probability of microcrack nucleation is skewed towards the positive values of θ when the crack is kinked to the upper plane (see Fig. 3.12). As discussed in the previous paragraph, the propagation direction is largely influenced by the presence of a damage cavity, and the crack propagates preferentially toward this ductile void. This mechanism results in a persistent process, and the Hurst exponent can be shown to take a value around $H \simeq 0.6$, larger than $1/2$ [18]. This process is similar to the quasi-brittle case presented previously where the nucleation of a microcrack ahead of the main crack tip results in persistency of the crack evolution.

To summarize, we have seen that roughness in a random microstructure is close to a random walk for which $H = 0.5$ but biased to a larger value $H > 0.5$ in the presence of damage. This is due to the tendency of cracks to continue growing, at least for a while, in the direction of damage. A more detailed investigation of the actual statistics of crack path in the presence of extensive damage is shown in the next section.

The role of extensive damage

To explore the effect of several micro-cracks on the crack trajectory, it is relevant to consider the random fuse simulations introduced in the previous Chapter. In the case of perfectly plastic fuses, the crack path was shown to be equivalent to a minimum energy path in a random network. In two dimensions, this is equivalent to the problem of the directed polymer in a randomly distributed potential [20]. The equilibrium configuration of the chain at zero temperature will be the one which minimizes the

energy along its path. This configuration is characterized by a well-defined roughness with exponent $H = 2/3$ [21]. Note that in three dimensions, the equivalent problem leads to a rough surface with exponent $H \simeq 0.42$ [22].

Seppala and coworkers' simulations [23] show that the perfectly brittle random fuse is very similar to the perfectly plastic case. In particular, the scaling properties of the simulated crack has a roughness exponent close to $2/3$, although there is only an overlap of 15% of the two crack paths. This equivalence between crack path and minimum energy line may be surprising since the minimum energy surface is a manifold at equilibrium. As a matter of fact, if a polymer can test all the configurations to finally choose the one which minimizes its energy, it cannot be the case of a crack, which is sensitive to the stress field in the vicinity of its tip only. As a consequence, and despite a roughness exponent similar to the minimum energy line, a description of the fracture process as a global minimization process seems unlikely.

References

- 1 Kertesz, J., Horvath, V., and Weber, F. (1993) Self-affine rupture lines in paper sheet. *Fractals*, **1**, 67–74.
- 2 Salminen, L.I., Alava, M., and Niskanen, K.J. (2003) Analysis of long crack lines in paper webs. *Eur. Phys. J. B*, **32**, 369–374.
- 3 Mallick, M., Cortet, P.P., Santucci, S., Roux, S.G., and Vanel, L. (2007) Discrepancy between sub-critical and fast rupture roughness: a cumulant analysis. *Phys. Rev. Lett.*, **98**, 255 502.
- 4 Salminen, L.I., Tolvanen, A.I., and Alava, M.J. (2002) Acoustic emission from paper fracture. *Phys. Rev. Lett.*, **89** (185503).
- 5 Stojanova, M., Santucci, S., Vanel, L., and Ramos, O. (2013) Statistical analysis of subcritical crack growth by acoustic emission vs. direct imaging.
- 6 Gol'dstein, R.V. and Salganik, R.L. (1974) Brittle fracture of solids with arbitrary cracks. *Int. J. Frac.*, **10**, 507–523.
- 7 Cotterell, B. and Rice, J.R. (1980) Slightly curved or kinked cracks. *Int. J. Frac.*, **16**, 155–169.
- 8 Katzav, E., Adda-Bedia, M., and Derrida, B. (2007) Fracture surfaces of heterogeneous materials: A 2d solvable model. *Eur. Phys. Lett.*, p. 46006.
- 9 Amestoy, M. and Leblond, J.B. (1992) Crack paths in plane situations - ii. detailed form of the expansion of the stress intensity factors. *Int. J. Solids Struct.*, **29**, 465–501.
- 10 Movchan, A.B., Gao, H., and Willis, J.R. (1998) On perturbations of plane cracks. *Int. J. Solids Struct.*, **35**, 3419–3453.
- 11 Maugis, D. (2000) *Contact, adhesion and rupture of elastic solids*. Springer.
- 12 Shabir, Z., Ponson, L., and Simone, A. (2011) Self-affine scaling of simulated intergranular cracks in brittle polycrystals, in *Proceedings of the Second International Conference on the Extended Finite Element Method – Partition of Unity Enrichment: Recent Developments and Applications – XFEM 2011* (eds S.P.A. Bordas, P. Kerfriden, and B.L. Karihaloo), Cardiff, UK.
- 13 Shabir, Z., Ponson, L., der Giessen, E.V., and Simone, A. ((Submitted)) Scaling properties of simulated intergranular fracture surfaces in brittle polycrystals.
- 14 Kachanov, M., Shafiro, B., and Tsurkov, I. (2004) *Handbook of elasticity solutions*, kluwer Academic Publishers.
- 15 Kachanov, M. (2003) On the problem of crack interactions and crack coalescence. *Int. J. Frac.*, **120**, 537–543.
- 16 Kachanov, M., Montagut, E.L.E., and Laures, J.P. (1990) Mechanics of crack-microcrack interactions. *Mech. Mat.*, **10**, 59–71.
- 17 Feder, J. (1988) *Fractals*, Plenum.
- 18 Bouchbinder, E., Mathiesen, J., and Procaccia, I. (2004) Roughening of fracture surfaces: the role of plastic deformation. *Phys. Rev. Lett.*, **92**, 245 505.
- 19 Bouchbinder, E., Mathiesen, J., and Procaccia, I. (2004) Stress field around arbitrarily shaped cracks in two-dimensional elastic materials. *Phys. Rev. E*, **69**, 026 127.
- 20 Roux, S. and Hansen, A. (1992) Perfect plasticity in a random medium. *J. Phys. II France*, **2**, 1007–1021.
- 21 Kardar, M. and Zhang, Y.C. (1987) Scaling of directed polymers in random media. *Phys. Rev. Lett.*, **58**, 2087–2090.
- 22 Middleton, A.A. (1995) Numerical results

for the ground-state interface in a random medium. *Phys. Rev. E*, **52**, R3337–3340.
23 Seppälä, E.T., Räsänen, V.I., and Alava,

M.J. (2000) Scaling of interfaces in brittle fracture and perfect plasticity. *Phys. Rev. E*, **61** (6), 6312–6319.